

## Structure of the Tubulin Dimer in Zinc-induced Sheets

T. S. BAKER AND L. A. AMOS

*Medical Research Council Laboratory of Molecular Biology  
Hills Road, Cambridge CB2 2QH, England*

(Received 16 February 1978)

The structure of tubulin has been studied in projection by minimum beam electron microscopy and image processing of negatively stained zinc-induced sheets. The reconstructed images include data to 15 Å resolution.

We report here a clear and reproducible 82 Å repeat arising from the arrangement of heterodimers in sheet aggregates of tubulin. This repeat is only observed in diffraction patterns from images recorded by minimum beam methods (10 to 20 e/Å<sup>2</sup>) and arises from small, but consistent, structural differences between two similar subunits believed to represent the two chemical species of tubulin monomer ( $M_r$ , 55,000). At higher electron doses (100 to 200 e/Å<sup>2</sup>), the additional information is lost or very much reduced, and only a repeat of 41 Å is observed, owing to the loss of distinction between monomers in the tubulin heterodimer.

The sheets are composed of 49 Å wide, polar protofilaments, similar to those observed in microtubules; however, the interprotofilament packing is completely different in the two structures. In these sheets, adjacent protofilaments point and face in opposite directions; i.e. they are related by dyad-screw axes normal to the protofilament axes and in the plane of the sheet. Thus, the zinc-induced sheets are crystals of space group  $P2_1$ , with cell dimensions of about 97 Å × 82 Å, containing one tubulin heterodimer per asymmetric unit.

Reconstructed images of four individual sheets, and their average, show the arrangement and shapes of the two heterodimers contained in each unit cell. The structure and packing of heterodimers in sheets are compared to those in opened out microtubules where all protofilaments point and face in the same direction.

### 1. Introduction

The occurrence of microtubules in a wide variety of eukaryotic cells is an indication of their importance in nature (for a recent review, see Snyder & McIntosh, 1976). The amino acid sequence of tubulin, the main constituent protein, appears to be highly conserved (Ludueno & Woodward, 1973). It would be of great interest to understand its structure in greater detail.

The arrangement of tubulin subunits in microtubules is now fairly well established, as a result of electron microscope studies of negatively stained flagellar and brain microtubules (Grimstone & Klug, 1966; Amos & Klug, 1974; Erickson, 1974a) and recent X-ray diffraction work on oriented hydrated specimens of brain microtubules (Cohen *et al.*, 1975; Mandelkow *et al.*, 1977). The microtubule wall is known to be made up of 13 longitudinal protofilaments, spaced at intervals of about 50 Å and each protofilament consists of a row of subunits spaced at intervals of about 40 Å. The

subunits in adjacent protofilaments are staggered by about 10 Å. These morphological subunits have been tentatively identified as tubulin monomers, since their volume appears to be consistent with the monomer molecular weight of 55,000. Tubulin occurs in solution as a 110,000  $M_r$  heterodimer of two polypeptide chains of similar molecular weight (Bryan & Wilson, 1971; Olmsted *et al.*, 1971; Luduena *et al.*, 1977) but rather different sequence, including at least 11 differences in the first 25 amino acid residues (Luduena & Woodward, 1973). One would therefore expect the 40 Å  $\times$  50 Å subunits to be paired in some way in the assembled microtubule. This is confirmed by clear evidence for an 80 Å longitudinal periodicity in optical diffraction patterns from electron micrographs of flagellar microtubules. This periodicity has been identified as a pairing of subunits along each protofilament (Grimstone & Klug, 1966; Amos & Klug, 1974). It is not usually evident in electron micrographs of brain microtubules (Erickson, 1974a); nevertheless, an 80 Å repeat is a consistent feature of X-ray diffraction patterns of brain tubules (Cohen *et al.*, 1975; Mandelkow *et al.*, 1977). It is likely that the 80 Å periodicity represents a fairly subtle difference in structure between adjacent subunits.

All the microtubules which have been isolated and studied in detail have been shown to contain other proteins in addition to tubulin. In the case of flagellar tubules, the numerous extra proteins (Linck, 1976; Piperno *et al.*, 1977) are believed to be responsible for a variety of longitudinal periodicities, all multiples of 80 Å, which are detected in optical diffraction patterns of electron micrographs (Amos *et al.*, 1976). The associated proteins of brain microtubules are much less readily detected in the structure; there is no evidence of contributions from them to the X-ray diffraction patterns. In the electron microscope, they are only observed in positively stained thin sections (Dentler *et al.*, 1975; Murphy & Borisy, 1975) or under optimum conditions of negative stain (Amos, 1977), as projections from the microtubule wall. However, the arrangement of projections appears to be based on a regular superlattice of 960 Å longitudinal repeat (Amos, 1977), suggesting that the associated proteins form some sort of a connective network over the tubulin lattice.

The resolution obtained in studies of microtubule substructure has so far been extremely limited. An analysis of the three-dimensional structure of flagellar microtubules from electron micrographs (Amos & Klug, 1974) was limited to about 40 Å resolution. The relatively low helical symmetry of the structure, which provides only 13 independent views of the repeating subunit in each image, results in serious difficulties in separating out contributions from the near and far sides of the cylinder. The results obtained, therefore, provided only a crude outline of the shape of the tubulin molecule. This limitation also applies to the reconstructed image of neuronal tubules presented by Tsuprun *et al.* (1975), where features smaller than 40 Å may not be very accurately reconstructed.

Higher resolution images of the tubulin subunits have come from studies of opened out tubulin sheets, which are observed, together with microtubules, under polymerizing conditions in preparations of microtubule protein from brain (Erickson, 1974a; Crepeau *et al.*, 1977). However, the possibility of extending the resolution beyond about 20 Å with such specimens is severely limited by the size of the sheets, which are seldom more than 10 to 13 protofilaments wide.

The assembly of tubulin into much wider sheets, in the presence of low (less than millimolar) levels of zinc ions was first reported by Larsson *et al.* (1976). Similar concentrations of magnesium ions appear to be essential for the assembly of normal

microtubules (Borisy *et al.*, 1975): when magnesium is replaced by zinc, abnormally wide sheets, usually consisting of 20 to 50 protofilaments, are formed. Such sheets provide much more favourable subjects for electron microscopic studies of the subunits. By averaging over large areas of a regularly repeating structure, the problems of radiation damage and low signal-to-noise ratios are reduced (Glaeser, 1971; Kuo & Glaeser, 1975). Crepeau *et al.* (1977) have studied the structure of zinc-induced tubulin sheets, both negatively stained and embedded in glucose, and have compared them with the "normal" sheets. They have shown that the arrangement of protofilaments is quite different in the two structures. Whereas the protofilaments in a sheet formed in the presence of  $Mg^{2+}$  all have the same orientation, those in a  $Zn^{2+}$ -induced sheet appear to alternate between two different orientations. However, the images were not sufficiently resolved to show the relationship between adjacent protofilaments, or to show a clear correspondence between subunits in the  $Zn^{2+}$ -induced sheets and those in the normal sheets. Nor was there any evidence of an 80 Å repeat along the protofilaments as might have been expected for well preserved specimens.

By analysing the projected structure of some exceptionally wide  $Zn^{2+}$ -induced sheets by minimum beam microscopy (Williams & Fisher, 1970; Unwin & Henderson, 1975), we are now able to demonstrate the polarity of the protofilaments and show that the sheets consist of antiparallel pairs of protofilaments. The subunits have a similar appearance to those in images of normal sheets. Furthermore, our images clearly show an 82 Å axial periodicity, which is manifested as a consistent difference in structure between adjacent subunits along each protofilament.

## 2. Materials and Methods

### (a) *Tubulin isolation, purification and sheet formation*

Microtubule protein was purified from bovine brain using the method of Shelanski *et al.* (1973). For details, see Amos (1977). After 2 purification cycles, the protein was sometimes stored at  $-20^{\circ}C$  in a buffer containing 50% glycerol, 20 mM-MES (2-[*N*-morpholino] ethane sulphonic acid), 0.5 mM-ethylene glycol-bis( $\beta$ -aminoethyl ether)*N,N,N',N'*-tetraacetate, 0.2 mM- $MgCl_2$ , 0.5 mM-GTP and used within five days. On other occasions the next stage was carried out immediately.

The tubulin sample was mixed with an equal portion of buffer containing 40 mM-MES and 1 mM-GTP, and microtubules were reassembled for 30 min at  $37^{\circ}C$ . The tubules were pelleted at 125,000 *g* for 1 h, rinsed with 40 mM-MES solution, resuspended in buffer at fairly high concentration (measured by the Lowry method as 5 to 10 mg/ml, or 0.05 to 0.1 mM in tubulin dimers), and depolymerized at  $5^{\circ}C$  for 30 min. This was spun at 65,000 *g* for 30 min and the supernatant solution retained for the formation of sheets. Polymerization of tubulin into sheets was induced by adding  $ZnSO_4$  to 0.25 mM and warming the sample to 30 to  $37^{\circ}C$ . Samples for electron microscopy were collected between 20 and 40 min after warming the solution.

### (b) *Electron microscopy*

Samples were diluted to 0.1 to 0.5 mg/ml in buffer (40 mM-MES, 1 mM-GTP, 0.25 mM- $ZnSO_4$ ), and applied to carbon-coated, 400-mesh copper grids for 30 s, either by normal adhesion (Huxley & Zubay, 1960) or by floating the grid face down on a 0.2-ml droplet of sample and, subsequently, slowly withdrawing the grid in a horizontal plane, leaving only a very thin film. Grids were then washed with a few drops of double-distilled water and stained for 30 s with 1% aqueous uranyl acetate. The result of the first method was that most sheets folded upon themselves and formed 2-layered structures (Fig. 1(c)). Grids prepared by the alternative procedure resulted in a majority of sheets attached to the carbon substrate in an unfolded configuration (Fig. 1(a)). Optical diffraction patterns

of unfolded sheets were noticeably better in quality than those from folded sheets. Reasons for this are unclear in view of previous reports which indicate the opposite tendency for 2-layered structures (Finch *et al.*, 1967; Aebi *et al.*, 1973). Perhaps strong interactions exist between the 2 surfaces in contact in the folded sheets and disrupt the regular structure, or the negative stain may interact differently with the double layer. Only unfolded sheets were included in the following analysis.

Minimum beam microscopy ( $\sim 20 \text{ e}/\text{\AA}^2$ ) was carried out at 80 or 100 kV with a Philips EM301 using essentially the same procedure as for imaging unstained specimens at very low electron doses ( $\sim 1 \text{ e}/\text{\AA}^2$ , Unwin & Henderson, 1975). In these experiments, the narrow, coherent, illuminating beam was produced by using 20  $\mu\text{m}$  first condenser and 100  $\mu\text{m}$  second condenser apertures, and a moderately excited (1.0 A) first condenser lens. A 30- $\mu\text{m}$  objective aperture aided in selection of a defocus sufficient to allow all spatial frequencies down to 10 to 15  $\text{\AA}$  to be recorded with phase contrast of the same sign (Erickson & Klug, 1971). Grids were scanned at 1900 $\times$  at an illumination level giving  $\sim 2.5 \times 10^{-2} \text{ e}/\text{\AA}^2$  per s at the specimen plane. An anticontamination device was used during minimal beam microscopy and also when minimum dose (10 to 20  $\text{e}/\text{\AA}^2$ ) and normal dose (100 to 200  $\text{e}/\text{\AA}^2$ ) images were recorded from identical specimen areas. Micrographs were recorded on Ilford Special Lantern Contrast plates and developed in Ilford PQ Universal developer.

Electron doses were estimated by calibrating the microscope exposure meter to Kodak 4489 Electron Image Film, exposed and developed under controlled conditions (Kodak Pamphlet no. P-198, Eastman Kodak Company, Rochester, New York, 14650). Two independent calibrations indicate that the exposure meter readings vary by less than 10%.

Our convention for microscopy was to place the specimen side of the grid facing away from the electron gun, so prints, made with the micrograph emulsion facing the enlarger light, present a view of the specimen through the carbon substrate.

Magnifications were calibrated from the 23  $\text{\AA}$  period of tobacco mosaic virus rods. Corrections were made to all measurements of dimensions, both in the images and their diffraction patterns, for a linear, electron optical distortion which gave rise to slightly anisotropic magnification (Baker, manuscript in preparation).

#### (c) *Optical diffraction*

The optical diffraction patterns of 138 zinc-tubulin sheets were screened in a surveying diffractometer (DeRosier & Klug, 1972), and patterns from well preserved areas (0.05 to 0.5  $\mu\text{m}^2$  at the specimen) of 48 sheets were recorded on 35 mm FP4 Ilford film. The number, intensity, sharpness, and lattice positions of the diffraction spots were the basis for the selection of 9 "best" images for digital processing. In addition, images were digitized only if the diffraction patterns showed prominent third layer-line ( $k = 3$ ) spots, were defocused such that the first minimum in the contrast transfer function (Erickson & Klug, 1971) fell outside the outermost observed reflections ( $d_{6,2} = 15 \text{\AA}$ , see Table 1), and showed little astigmatism.

Patterns were recorded with the micrograph emulsion toward the laser. The diffraction patterns in Figure 2 correspond with the orientation of the sheet in Figure 1(b).

#### (d) *Digital processing*

Only images recorded by minimal beam microscopic methods were used for image reconstruction. 0.05- $\mu\text{m}^2$  areas, containing  $\sim 650$  unit cells, were microdensitometered (Arndt *et al.*, 1968) at the equivalent of 4.4  $\text{\AA}$  intervals, and the resulting  $512 \times 512$  arrays were transformed on an IBM 370/165 computer. The digital transforms usually contained additional reflections not observed in the optical patterns. Five images were selected from the 9 densitometered arrays according to similar criteria to those used in screening the optical transforms. In each case, out of 63 possible reflections within a 15  $\text{\AA}$  limit, those which were not clearly evident as peaks above the background were eliminated from the data. Single amplitudes and phases for each remaining reflection were determined by several methods, all giving similar results. The method in this report was first to fit the best reciprocal lattice grid to the positions of the strongest 24 peaks in the transform, thereby defining exact positions for all of the lattice points. The phase at each ideal lattice

point was calculated by bilinear interpolation of the structure factors of the 4 surrounding sample points in the digital transform. Amplitudes were computed as the root-mean-square amplitude of all sample points within a small radius (a distance of 2 sample points in this case) of the lattice position. (The intensity sum was divided by the number of sample points, since the number included in the circle varied slightly.) This method was used because some of the diffraction spots in each transform appeared to be split into 2 or more peaks around the ideal lattice point, which might lie on a minimum between 2 such peaks. By integrating around the lattice point, slightly irregular images can be "restored". Weak, split reflections are thus given slightly higher weighting than if an interpolated value exactly at the lattice point were calculated. No attempt was made to correct for background noise in the diffraction patterns. It was assumed that most of this would be eliminated by averaging data from different images. Also no correction was applied for the expected falloff in amplitudes at the high orders due to phase contrast effects (Erickson & Klug, 1971).

Reconstructed images (Fig. 3(a) to (d)) were computed in space group  $P1$  (assumes no symmetry) with a crystallographic Fourier summation program written by George Reeke Jr, and the results displayed as contoured density plots on a CALCOMP model 1136 plotter attached to the IBM 370/165 via a model 900 controller. To facilitate interpretation, positive (red) and negative (green) contours are plotted in different colours so black and white transparencies can discriminate the two. Since the central reflection ( $h = 0, k = 0$ ) was not included in any of the reconstructions (see footnote to p. 114), the average amplitude is exactly zero in each, with the first dark contour at zero and all other dark lines representing positive peaks and light lines, negative peaks.

The data from these 5 images were then compared. The images were readily oriented the same way up by comparison of the phases of the corresponding Fourier terms. Approximate common phase origin positions were determined in the following way: the origin in each image was placed along the axis of one of the protofilaments by setting  $\phi(2,0) = 0^\circ$ . It was then shifted along this axis (i.e. parallel to the protofilament) until it approximately coincided with a selected screw axis (see legend to Table 1).

With the image in Figure 1(a) as reference, the phase origins of the other 4 "best" images were refined to give the best overall agreement among the phases at each lattice point. This was determined using a least-squares procedure, with the phase difference for each reflection weighted by the average amplitude. Excellent phase agreement for most of the reflections (see Table 1) was found among 4 of the 5 images. The fifth was rejected at this stage since the phases of some of the higher resolution reflections did not agree with those of the other examples.

The data from the 4 remaining images were combined to give an average reconstruction. Initially, this was done without enforcing  $P2_1$  symmetry on the data. To suppress any bias from a particular example, the diffraction amplitudes were first multiplied by a scaling factor, chosen so that the mean intensity of the reflections in each diffraction pattern was the same. To ensure the quality of all the data, any reflection for which the root-mean-square difference in the individual phases exceeded  $40^\circ$  was discarded. Furthermore, the method of averaging, by vector summation of the real and imaginary parts of each Fourier term, ensured that reflections with large standard deviations in phase would have least influence on the final result. With these constraints, 32 reflections, illustrated in Figure 2(a), and listed in Table 1, were included in the average reconstruction, which was computed and displayed as given above.

A final average reconstruction, with a perfect dyad screw axis, was computed after correcting the amplitudes and phases in Table 1 so that they obeyed the symmetry rules exactly.

### 3. Results

#### (a) *Formation of tubulin sheets*

Wide (50 to 200 protofilaments) sheets (up to  $1 \mu\text{m}^2$ ) were obtained only when moderately high concentrations of tubulin (5 to 10 mg/ml) were incubated in the

presence of 1 mM-GTP and 0.25 mM-Zn<sup>2+</sup>, at 30 to 37°C. However, in some experiments these conditions led, instead, to production of narrow (<50 protofilaments) sheets, which were always obtained at lower tubulin or zinc concentrations. Sheets, whether wide or narrow, were generally 1 to 2 μm long and gave identical diffraction patterns. We also tested the effects of other divalent cations, Co<sup>2+</sup>, Cu<sup>2+</sup> and Ni<sup>2+</sup> (Wallin *et al.*, 1977), but were not able to induce the formation of large sheets with these ions.

### (b) *Electron micrographs*

Figure 1(a) illustrates an image of a typical, negatively stained, "large" sheet. The major feature in such images is the characteristic protofilament structure, with neighbouring strands approximately 50 Å apart (see Fig. 1(b)). Each protofilament is subdivided into domains with an approximate 40 Å spacing which gives rise to the two other noticeable striations in unprocessed images; these striations are easier to visualize if the sheet is viewed at a glancing angle in a direction approximately 65° from either side of the protofilament direction. The structure and arrangement of the protofilaments in the sheets, and their relation to other microtubular structures, are not obvious from inspection of the unprocessed images.

### (c) *Diffraction patterns*

Figure 2(a) illustrates a typical optical diffraction pattern from a minimum exposure image of a well preserved sheet. Such patterns contain a wealth of information not apparent in the images, and reveal much about the underlying structure which can be confirmed by computing filtered images (see section (d), below). Images recorded with no precaution to limit radiation levels gave inferior patterns, as illustrated by the differences between Figure 2(b) and (c).

The patterns confirm the observations of Larsson *et al.* (1976) and Crepeau *et al.* (1977) that the subunit lattice is different from the surface lattice of opened out microtubules. Although the major intensities lie on layer-lines with a fundamental meridional repeat of about 40 Å in both cases, the positions of the peaks along the layer-lines are different. In patterns from normal sheets (Erickson, 1974a; Crepeau *et al.*, 1977), the reflection nearest to the meridian on one side is much closer than that on the other side (these peaks correspond to the third and tenth order Bessel reflections, respectively, in microtubule diffraction patterns), whereas diffraction patterns from zinc-induced sheets show reflections equally spaced about the meridian (Crepeau *et al.*, 1977).

Diffraction from our sheets reveals a striking *mm* symmetry (i.e. both the meridian and equator are mirror lines). An intensity distribution of this type is characteristic of a structure containing at least one dyad axis in the plane of the structure and parallel to either the equatorial or meridional direction. For a two-dimensional crystal, the *mm* symmetry also implies that the unit cell is orthogonal (rectangular). Most of the measured angles ( $\gamma^*$ , see Fig. 2(a)) differed by a few tenths of a degree from 90°. However, it was shown (Baker, manuscript in preparation) that the major cause of these departures from orthogonality was a 1.7% distortion in the imaging system of the microscope. After correction for this distortion,  $\gamma^*$  avg = 89.9 ± 0.4°.

In addition to the central spot (0,0), the equator contains up to three unique reflections, whose positions reflect the 49 Å spacing between adjacent protofilaments.

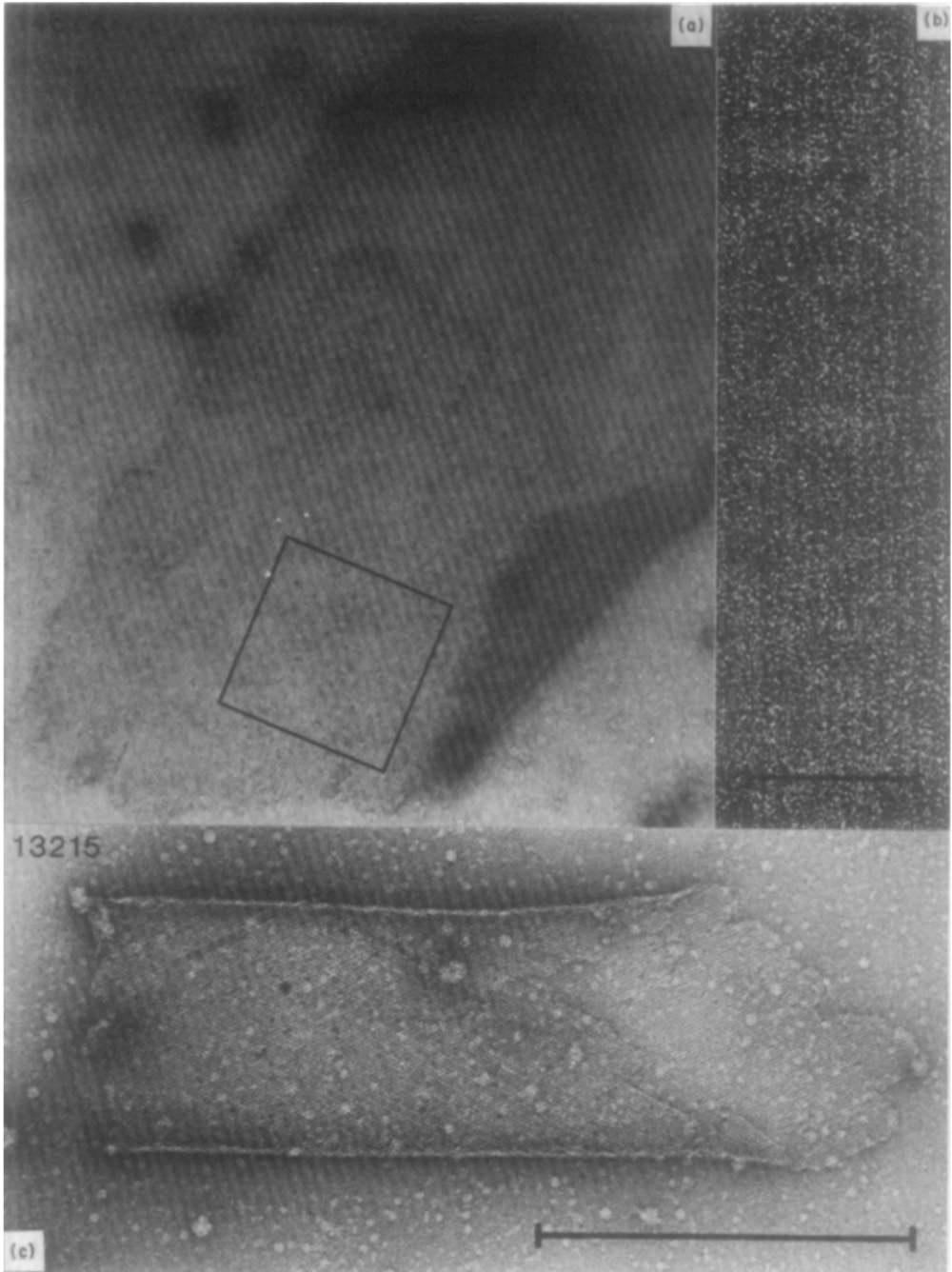


FIG. 1. Electron micrographs of zinc-induced tubulin sheets, negatively stained in 1% aqueous uranyl acetate and recorded with minimal electron doses (typically  $\sim 20$  e/Å). Protein appears white and stain black in these positive images.

(a) An unfolded tubulin sheet. The outlined region represents the specimen area digitized as a  $512 \times 512$  array, and contains over 600 unit cells of dimensions  $97 \text{ \AA} \times 82 \text{ \AA}$ . Magnification as for (c).

(b) Enlarged region of (a) showing prominent vertical striations corresponding to the division of the structure into protofilaments. Magnification bar represents  $500 \text{ \AA}$ .

(c) Tubulin sheet folded upon itself. The criss-cross pattern of striations arises from the superposition of protofilaments in the overlapping layers. The angle of overlap is approximately  $40^\circ$ . Magnification bar represents  $0.5 \text{ \mu m}$ .

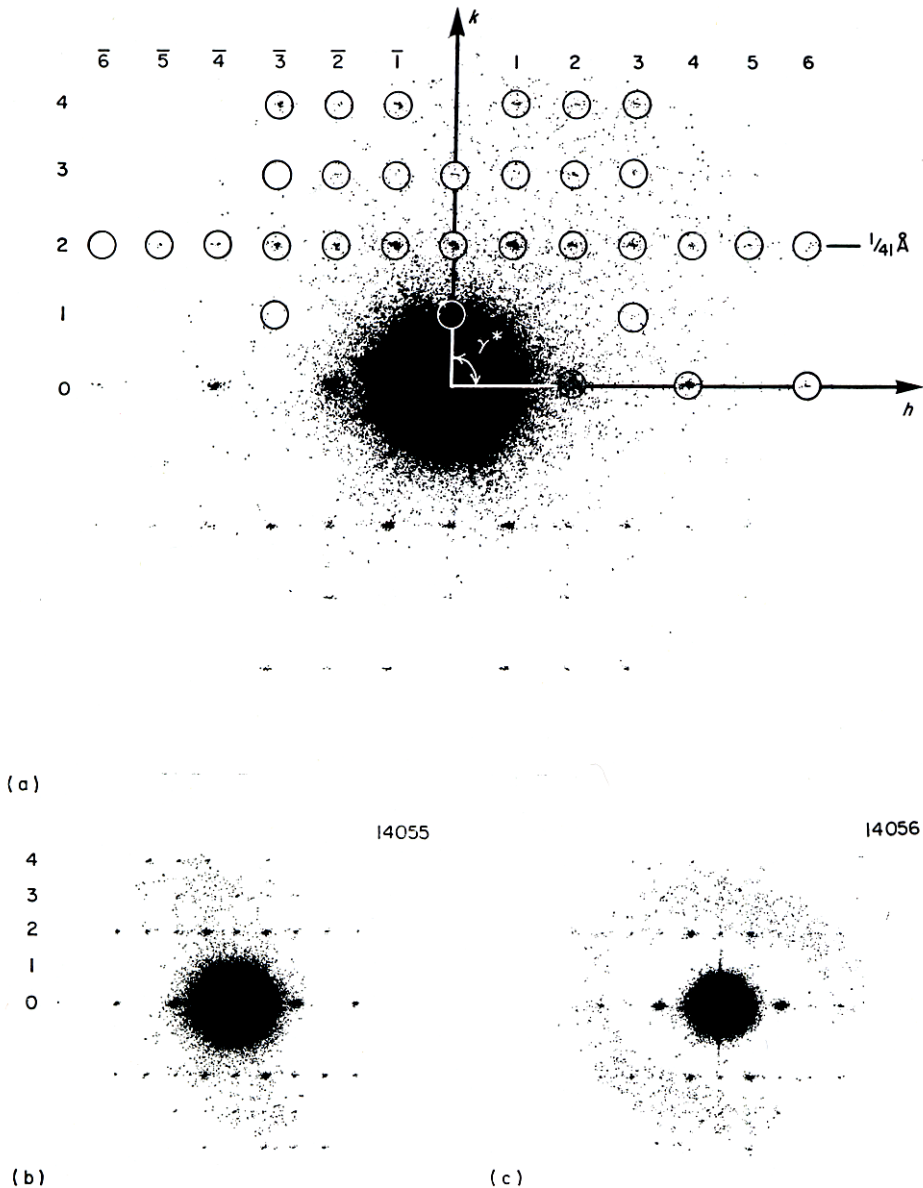


FIG. 2. Optical diffraction patterns from circular regions of zinc-induced tubulin sheets (protofilaments oriented vertically).

(a) Pattern from an area containing  $\sim 2500$  unit cells of the image in Fig. 1(a). The equatorial and meridional axes are labelled  $h$  and  $k$ , respectively. Note that the intensity distribution obeys a near perfect  $mm$  relationship (i.e. each spot has 2 mirror-related mates reflected across the  $h$  and  $k$  mirror lines). An orthogonal reciprocal lattice, with a  $1/82 \text{ \AA}^{-1}$  axial repeat and a  $1/97 \text{ \AA}^{-1}$  equatorial repeat, is an obvious choice for indexing the pattern. The circled reflections illustrate those data (Table 1) taken from each of the individual images and included in the average reconstruction (Fig. 3(e)).

(b) Pattern from an image recorded at  $\sim 20 \text{ e/\AA}^2$ . The 3rd and 4th layer-line spots are clearly visible, as are the higher orders on the 2nd layer-line ( $k = 2$ , with  $h > 3$ ) and the (6,0) spot on the equator. The slight asymmetry in the intensity distribution, which violates the  $mm$  symmetry, results mainly from residual astigmatism in the image.

(c) Pattern from the identical area of a second image of the same sheet in (b), recorded at  $\sim 200 \text{ e/\AA}^2$ . Note the overall poorer quality compared with (b) and especially the virtual absence of 3rd layer-line spots, which provide information necessary to define the tubulin heterodimers.



Since the other layer-lines reveal a basic equatorial spacing of about 97 Å (see below), it is clear that alternate spots are absent from the equator. Thus, the dyad screw axis mentioned above must be normal to the protofilament axes. This result has been confirmed by the phase relationships in the computed Fourier transforms (see Table 1). Thus, each protofilament is related to its nearest neighbours by a rotation of 180° about the screw axis and a translation of 49 Å along the same screw axis. This means that protofilaments are not physically grouped sideways into pairs because the bonding pattern of a given protofilament is equivalent with both adjacent protofilaments.

The pattern indexes in the axial direction on an 82 Å repeat. The 41 Å (second) layer-line contains as many as 13 spots, positioned at 1/97 Å intervals, which is equivalent to the spacing between alternate protofilaments. The 20 Å (fourth) layer-line is the other prominent, non-equatorial layer-line and contains up to eight reflections with the same 1/97 Å spacing.

A less prominent but consistent feature of the diffraction patterns from our specimens is a 27 Å (third) layer-line positioned midway between the second and fourth layer-lines. A maximum of seven, particularly radiation-sensitive (Fig. 2(b) and (c)) spots, spaced at 1/97 Å, in positions consistent with the lattice revealed by the other three layer-lines, have been observed along this line, which appears in most of the patterns from images of large sheets recorded by minimal beam methods. Its presence requires the axial repeat (along the protofilament) to be at least 82 Å. A first layer-line might also be expected to appear in the diffraction patterns. Occasionally, a few spots are seen, and digital processing reveals three weak reflections (−3,1; 0,1; and 3,1) consistently present in the four “best” images. Because these are so weak, though, they contribute little noticeable difference to the reconstructed images. No additional reflections were ever identified beyond the fourth layer-line.

#### (d) *Reconstructed images*

Reconstructions (Fig. 3(a) to (d)) of the four “best” images (selected on the basis of their optical and digital diffraction patterns), and their combined average (Fig. 3(e)) were computed (Materials and Methods, section (d)). A total of 32 independent reflections were included in the average (see Table 1); some of the individual reconstructions included a few additional reflections.

Obvious differences distinguish the four reconstructed images. However, several common features are recognized, and are easier to understand by comparing the individual images to the average in Figure 3(e). Here, one unit cell (97.4 × 81.8 Å) is outlined, with the phase origin chosen to lie where one of the screw axes crosses a protofilament axis. A unit cell contains four elongated subunits, each of whose integrated density within the zero contour is the same to within 10%. Each subunit corresponds roughly in size to the 55,000 molecular weight tubulin monomer (Amos & Klug, 1974). The two adjacent protofilaments contributing to a 97 Å sideways repeat are referred to as PFI and PFII. The subunits along each protofilament alternate in appearance and are labelled  $\alpha$ I and  $\beta$ I in PFI and  $\alpha$ II and  $\beta$ II in PFII. It is clear that, although the screw relationship has not been enforced, in each image  $\alpha$ I is very similar to the mirror image of  $\alpha$ II, and  $\beta$ I is similarly related to  $\beta$ II. The long axes of  $\alpha$ I and  $\beta$ I are tilted up and to the left by 40 to 50° from the PFI axis, and  $\alpha$ II and  $\beta$ II are tilted up and to the right by 40 to 50° in PFII.

TABLE 1

*Data on reflections contributing to the average reconstructed image*

$h$	$k$	Amplitude	$\phi$	Root-mean-square deviation	$\phi'$	$\phi''$	$(h', k')$	$d$ (Å)
2	0	877	0	1	0	0	(2,0)	48.7
4	0	250	236	4	210		(4,0)	24.4
6	0	106	30	10				16.2
-3	1	65	122	24				30.2
0	1	78	12	16†				81.8
3	1	68	42	10†				30.2
-6	2	59	115	37				15.1
-5	2	67	340	29				17.6
-4	2	99	300	11				20.9
-3	2	141	220	4				25.4
-2	2	143	76	8	120	100	(-3,1)	31.3
-1	2	309	202	5	195	225	(-2,1)	37.7
0	2	158	8	9	50	20	(-1,1)	40.9
1	2	295	338	4	345	315	(0,1)	37.7
2	2	127	296	7	190	310	(1,1)	31.3
3	2	130	329	12	305		(2,1)	25.4
4	2	83	45	22				20.9
5	2	77	192	25				17.6
6	2	66	244	23				15.1
-3	3	68	329	16†				20.9
-2	3	85	220	20				23.8
-1	3	75	224	11				26.3
0	3	96	4	7				27.3
1	3	67	311	23				26.3
2	3	85	131	7				23.8
3	3	69	242	13				20.9
-3	4	116	117	10				17.3
-2	4	85	277	20				18.9
-1	4	117	355	7	5		(-3,2)	20.0
1	4	102	185	10	145		(-1,2)	20.0
2	4	71	70	16				18.9
3	4	92	64	21				17.3

Data for the 32 reflections that contributed to the average reconstructed image. Indices ( $h, k$ ) are as defined in Fig. 2(a). Amplitudes are on an arbitrary scale, and phases ( $\phi$ ) are given in degrees, relative to a phase origin at the intersection of a PFI protofilament axis and one of the proposed dyad screw axes (see Fig. 3(e)). For perfect data the phases would be related so that  $\phi(h, k) + \phi(-h, k) = h\pi$ . The departures from this rule are smaller than the corresponding phase errors shown in the fifth column, which lists the root-mean-square differences in the phases of the 4 images contributing to the average, thus providing a measure of the accuracy of the average data.

For comparison, the relative phases obtained by Crepeau *et al.* (1977) (after an inversion and shift of phase origin), on stained ( $\phi'$ ) and unstained ( $\phi''$ ) material, are listed, together with the indices ( $h', k'$ ) used in their analysis. The poor agreement between their stained image and both our stained image and their own unstained image arises mainly from the differences in phases for the (-2,2) and (2,2) reflections. This is possibly a staining artifact. Their data do not include any 82 Å or 27 Å layer-line information, although they state they have used minimum beam methods to record their images. Part of the reason might be that they processed smaller areas ( $\times 4$ ), which would lead to a 2-fold reduction in the signal-to-noise in all reflections. Furthermore, since the 82 Å information is variable in strength, even within a single digitized area, it may be that the areas chosen were unfavourable in this respect.  $d$  (Å) gives the spacing corresponding to each reflection.

† Present in only 2 or 3 of the 4 computed transforms.

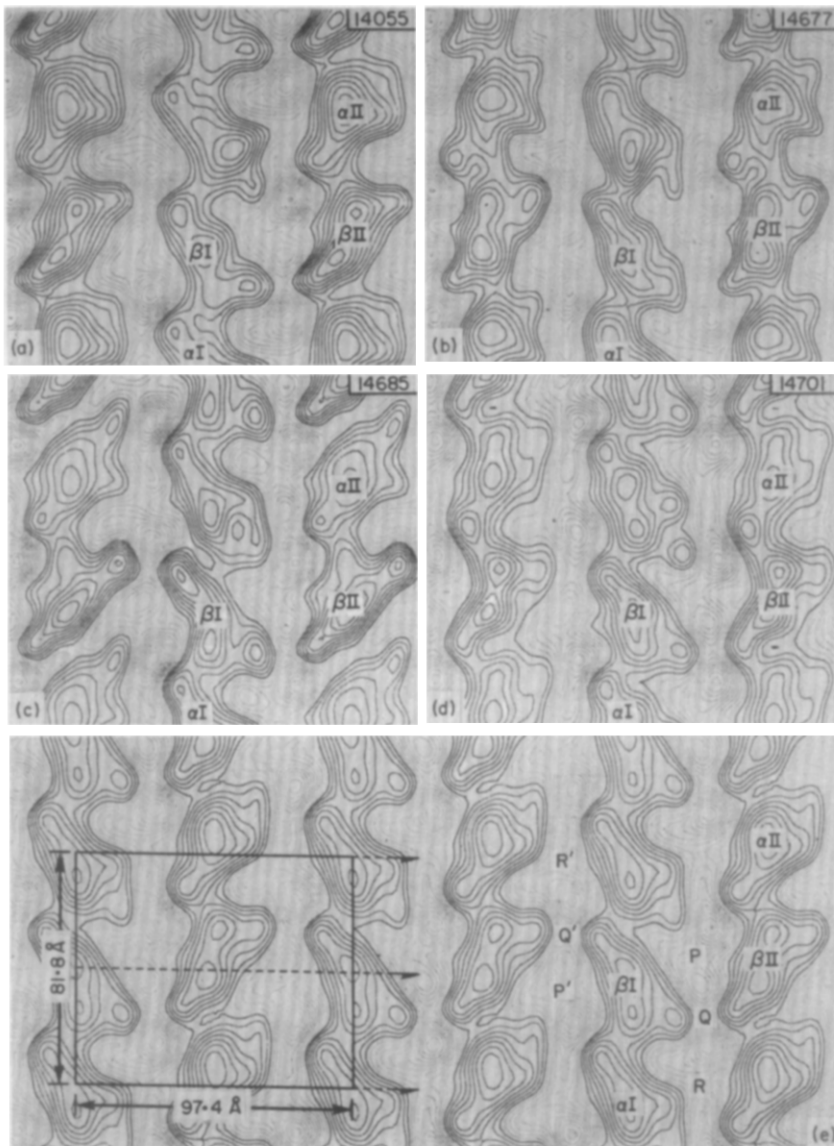


FIG. 3. Image reconstructions of 4 individual sheets and their average. Dark lines represent contours of density from zero to successively higher positive amplitudes. Light lines represent contours at negative amplitudes. See Materials and Methods, section (d), for details.

(a) to (d) Individual reconstructions from 4 images, showing corresponding regions of the structure. The subunits are labelled to indicate the possible pairing of monomers into heterodimers, and to show the relationship of dimers in adjacent protofilaments. The  $\alpha$  and  $\beta$  labels are arbitrary and do not indicate known identities for the chemically distinct species of tubulin monomer. Type I subunits slope upwards to the left and type II in the opposite manner.

(e) Average reconstruction of the 4 sheets (a) to (d), showing the contents of several unit cells. One cell is outlined, and the positions of the proposed dyad screw axes are indicated by the broken lines with half-arrows. Note, however, that in this reconstruction (and also in (a) to (d)) the structure is not forced to contain a perfect screw axis. P, Q and R indicate possible points of interprotofilament contacts between the right side of a type I protofilament (PFI) and the left of a type II (PFII). P' Q' and R' are the equivalent contacts between the left side of PFI and the right of PFII.

Obviously, PFI and PFII may be regarded as face-up and face-down views of the same structure. Two unique screw axes, indicated by the broken lines with half-arrows in Figure 3(e), relate adjacent protofilaments. If one protofilament is fixed and the other rotated through  $180^\circ$  about either of the dyad axes, and then translated along this axis by one-half of the cell ( $49 \text{ \AA}$ ), the mass distributions in the two protofilaments almost perfectly superimpose. When the averaged data are constrained to obey a perfect screw axis, an averaged image of the two protofilaments in Figure 3(e) is obtained, which has been incorporated in Figure 4(a).

It is assumed that the differences in shape between  $\alpha$  and  $\beta$ -type subunits in some way reflect the chemical differences between the two different species of tubulin monomer (Ludueno & Woodward, 1973). (The labels were chosen to be consistent with those of Amos & Klug (1974), see Discussion, and may or may not correspond to the chemical notation.) There are two types of intraprotofilament connections between subunits, both on the left side of each protofilament. One is more dense than the other, implying a stronger or more extensive intersubunit contact region, and might be the contact responsible for the formation of tubulin heterodimers. This pairing is especially evident in Figure 3(c) and is indicated in each reconstructed image by the labelling scheme. A consequence of the sidedness in the positions of the intraprotofilament subunit contacts is the rather smooth contour of the left side of each protofilament and the highly indented appearance of the right side. This presumably reflects the surface structure of the protofilaments, with the right side of each protofilament containing larger pockets where stain accumulates.

The projected density between protofilaments contains some strongly negative regions, which probably contain very little protein. Between these deeply stained regions are zones of significantly higher density which presumably represent positions of interprotofilament contact $\dagger$ , although the density here is much lower than that of the intraprotofilament contacts discussed above. There are three points of apparent close contact (P, Q, R, Fig. 3(e)) between adjacent protofilaments. The closest contact appears to be between  $\beta$ I and  $\beta$ II (Q, Q'). R and R' are possible contacts between the two alpha subunits, while P and P' could either be  $\alpha$ I- $\beta$ II or additional  $\beta$ I- $\beta$ II contacts (or both).

#### 4. Discussion

The tubulin structure we have studied is abnormal, in the sense that it occurs only in the presence of zinc ions. Nevertheless, we believe it to be closely related to the normal microtubule structure, since it consists of protofilaments similar to those in microtubules and viewed from a similar angle, but arranged side by side in a different way. One reason for believing in this similarity is that both the interprotofilament ( $48$  to  $49 \text{ \AA}$ ) and intraprotofilament ( $40$  to  $41 \text{ \AA}$ ) spacings are identical to those in sheets polymerized without zinc, which are believed to be opened out microtubules (Erickson, 1974a). If there were a substantial rotation between the two views, one would expect this to be reflected in a significant change in interprotofilament spacing,

$\dagger$  Boundaries and contacts cannot, of course, be determined exactly in negative stain, since "absence of stain" cannot be measured on an absolute scale unless the object is in a perfectly uniform layer of stain. However, a higher density at particular points along the interprotofilament region must imply more extensive, and presumably stronger, intersubunit contacts at these points.

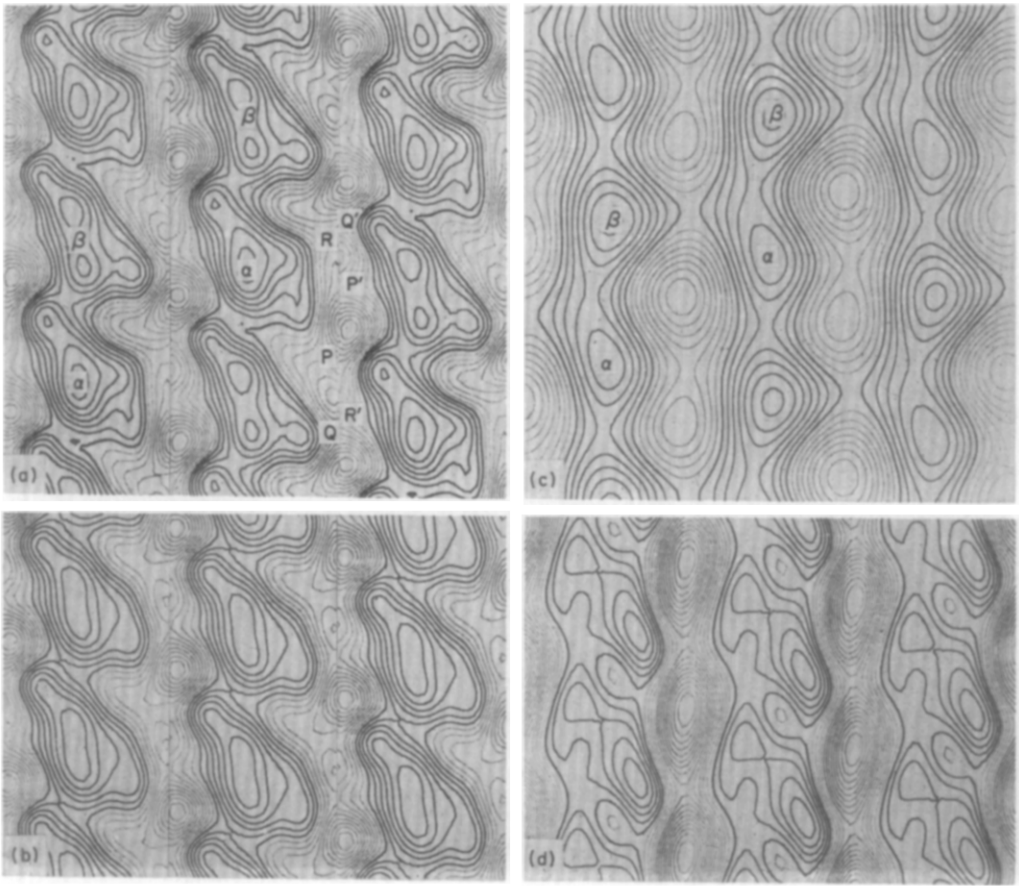


FIG. 4. (a) Images of the averaged zinc-tubulin dimer, arranged on the "normal" opened microtubule lattice, (see Fig. 5), as viewed from the equivalent of the outside surface of a microtubule. The averaged image was obtained by imposing a 2-fold screw axis on the data used to produce Fig. 3(e). With all the protofilaments in this orientation, the images fit together naturally into the normal tubulin lattice as viewed from the outside surface. To produce the less likely alternative arrangement mentioned in the text, adjacent protofilaments would have to be shifted relative to one another by about 20 Å in the axial direction to lie on a lattice which is the mirror of the one shown here. This would then correspond to a view from the inside surface. The result would be that regions of lowest density on one side of the join would lie next to regions of much higher density on the other side. Also, the slope of the subunits relative to the lattice directions would be opposite to that in normal sheets.

(b) Similar to (a) except that data from the 1st ( $k = 1$ ) and 3rd ( $k = 3$ ) layer-lines were omitted, so that each subunit is now an average of  $\alpha$  and  $\beta$ .

(c) A radial projection of a very low resolution reconstructed image of flagellar microtubules obtained by Amos & Klug (1974), which includes data from an 82 Å layer line. The labelling of  $\alpha$  and  $\beta$  corresponds to their labelling, which was chosen arbitrarily. The difference in density between  $\alpha$  and  $\beta$  subunits is probably a staining artifact. Note the greater intraprotofilament density between the labelled pairs of subunits compared with that between different dimers. The image shown here is oriented so that the top is towards the basal end of a flagellum.

(d) Reconstructed image of an opened out microtubule, replotted from the data of Crepeau *et al.* (1977). The zero contour level has been slightly shifted upwards to show more clearly the oblique, intraprotofilament cleft between subunits.

since the protofilaments are apparently 70 to 80 Å wide in side view, as measured from the microtubule wall thickness (Mandelkow *et al.*, 1977). The average interprotofilament spacing in microtubules themselves is slightly larger (53 Å) than in either kind of sheet, although the axial spacing ( $40.5 \pm 1.0$  Å) is the same (Mandelkow *et al.*, 1977). This probably means that the bonds between protofilaments are not at the mean radius of the microtubule wall, but towards the inside.

Our results show protofilaments arranged in the zinc-induced sheets in a specific antiparallel configuration. Thus, the interprotofilament bonding between monomers is unlike that of any other known tubulin aggregate. This arrangement is verified by the *mm* symmetry in the intensity distribution of the diffraction patterns, along with the absences on the equator, and is clearly represented in the reconstructions (Fig. 3) where no symmetry was imposed. Obviously this result depends to some extent on studying sheets which are nearly equally stained on both sides. The very thin layers of uranyl acetate in which our specimens were embedded appear to be ideal in this respect.

The protofilaments are revealed as distinctly polar structures, consisting of wedge-shaped subunits with their axes tilted 40 to 50° away from the protofilament axes. The polarity is a strong feature; as can be seen from Figure 4(b), it is quite independent of the weak odd layer-line information. Within each protofilament there are two distinguishable subunits, which we identify with the two species of (55,000  $M_r$ ) tubulin monomers, paired into heterodimers. Our observation of a distinction between these two subunits depends solely upon the information contained on the odd layer-lines. As these two subunits are roughly equivalent in size and gross morphology, and because the ability of the stain to reproduce a faithful outline of the subunit shape is highly radiation-dependent (Unwin, 1974), it is not surprising that these small details are easily lost. In addition, inspection of digitally filtered images (not shown), where the averaging was only over local rather than entire regions, indicated that these details may not be preserved over all parts of a single sheet image.

It is necessary to consider possible contributions to the images from microtubule-associated proteins (Sloboda *et al.*, 1975) especially the high molecular weight proteins (Borisy *et al.*, 1975). The Zn-sheets were assembled in protein solutions containing not only tubulin but also 15 to 25% high molecular weight proteins (see Amos, 1977). We are not sure that the latter are incorporated into the sheets, since Gaskin & Kress (1977) found that purified tubulin polymerized alone, after addition of zinc ions. There is no indication in the diffraction patterns of periodicities larger than 82 Å in the axial direction that one might attribute to non-tubulin components, but this does not prove their absence. Most of the high molecular weight molecule takes the form of a filamentous projection from the wall of a normal microtubule. If these molecules behave similarly in the Zn-sheets, the projections are probably flattened and very distorted; they will therefore be filtered out of the reconstructed images. Probably about 10% of the molecule is directly bound to tubulin (Vallee & Borisy, 1977) and this part would make a more definite contribution to the filtered image. However, 10% of  $\sim 300,000 M_r$  averaged over 12 dimers (see Amos, 1977) would add less than 3% to the mass of each dimer, therefore it would not contribute much to the reconstructed image. Still, it might account for part of the observed structural difference between  $\alpha$  and  $\beta$ .

In Figure 4(a) we show images of the fully averaged protofilament, lined up in the same orientation, and arranged on the lattice of an opened out microtubule. Figure 5

illustrates this transformation diagrammatically. For reasons discussed above, we assume that the transformation involves little or no rotation of the protofilaments about their long axes. The regions of contact between subunits in this arrangement correspond closely to those in the original sheet (Fig. 3(e)), although they are matched up differently. In the alternative arrangement, that is with the mirror view of the protofilaments arranged on the same lattice, these bonding regions would not match up, nor would the shape of the subunits agree with that in normal tubulin sheets (Fig. 4(d)). It therefore seems highly likely that the images in Figure 4(a) correctly represent the outside view of the protofilaments. Figure 4(b) shows the effect of omitting the first and third layer-line information from the reconstructed image. Reconstructed images from flagellar microtubules (Amos & Klug, 1974) and normal tubulin sheets (Crepeau *et al.*, 1977) are shown alongside for comparison.

Resolution in the flagellar tubule reconstruction (Fig. 4(c)) is too low to reveal clearly any definite shape in the subunits. However, the 82 Å information contributes to a certain polarity in the image. We have therefore oriented the image with the less indented side of the protofilaments to the left, to agree with Figure 4(a). The labelling of  $\alpha$  and  $\beta$  in Figures 3(a) to (e) and 4(a) was chosen so that the denser intraprotofilament connections would also be the same in the two structures. Even with this criterion, we cannot, of course, be sure that the labelling is consistent.

Similarly, Crepeau *et al.*'s normal sheet image is shown (Fig. 4(d)) in what seems to be the best relative orientation. There is a discrepancy in that the average density is stronger on the left side of the Zn-tubulin protofilaments, but on the right side of the normal tubulin protofilaments (i.e. the 25 Å equatorial reflections are out of phase). However, this could probably arise from a small rotation of protofilaments between the two structures.

It may also be appropriate here to compare the reconstructed images of Zn-induced sheets obtained by Crepeau *et al.* (1977) with ours. (The similarities and differences are summarized by the phase information presented in Table 1.) Although their data do not contain information pertaining to an 82 Å meridional repeat, the reconstruction of our stained sheets (Fig. 3(e)) agrees well with their reconstruction of unstained sheets (Fig. 9 of Crepeau *et al.*, 1977). The elongated subunit shapes and their opposite tilt in adjacent protofilaments are clearly evident in both reconstructions. Their reconstruction of stained sheets (Fig. 8 of Crepeau *et al.*, 1977), on the other hand, does not compare well with either of these reconstructions, showing little evidence of polarity. Only one of the two kinds of protofilament shows a suggestion of elongated subunits, whereas in adjacent protofilaments, the subunits appear more globular and display no apparent skewing. The reason for these differences is not understood, but an asymmetric staining may be partly responsible.

Allowing for the lack of resolution in the flagellar microtubule image and the absence of the 82 Å repeat in the normal sheet image, the correlation between our images of Zn-tubulin protofilaments and normal Mg-tubulin protofilaments is quite good. The agreement provides added support for our assumption that the view of the protofilaments is very similar in both the normal and zinc-induced sheets. It seems that protofilament structure is largely independent of which cation ( $Mg^{2+}$  or  $Zn^{2+}$ ) is added to the solution for assembly. Comparison of Figures 3(e) and 4(a) suggests that no significant change in internal structure of the protofilament is necessary in the transformation from one assembly form to the other (cf. Fig. 5(a) and (b)). The added ions appear to act specifically in determining the interprotofilament bonding. From

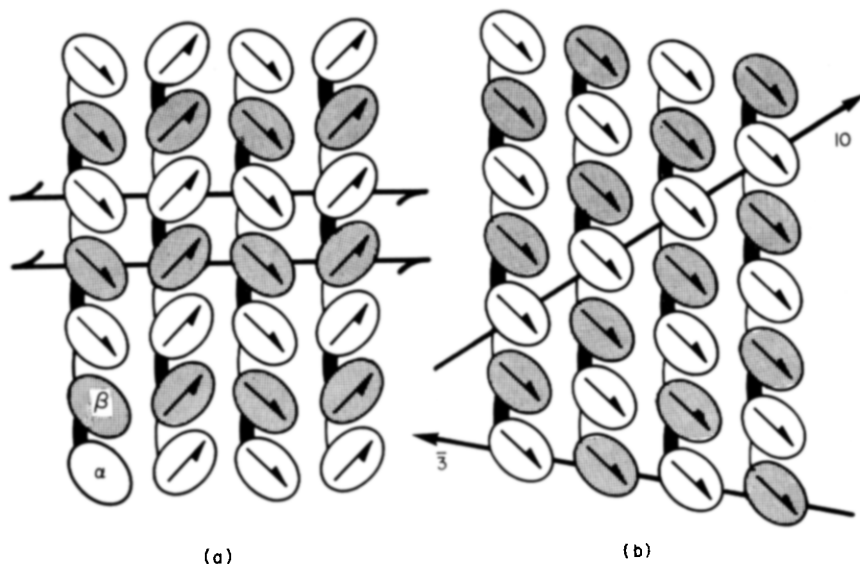


FIG. 5. Schematic drawings of the packing of protofilaments in Zn-induced sheets and opened microtubules. Subunits are shaded to distinguish the 2 monomer species and the contacts responsible for heterodimer pairing are indicated by the thicker intraprotofilament connections. The half-arrows in each monomer indicate subunit polarity and orientation.

(a) Zn-induced tubulin sheet packing: 2 dyad screw axes are drawn, showing the relative orientation of protofilaments. The centre of mass in each monomer is shown slightly shifted away from the screw axis to correspond with the reconstructed images (Fig. 3). Note that the subunits in adjacent protofilaments are viewed from opposite sides. The closest interprotofilament connections are between monomers of the same type.

(b) Packing in an opened "normal" microtubule, viewed from the equivalent of the outside of the tubule. The directions of the 3- and 10-start helical families are indicated. All the protofilaments are similarly oriented. The arrangement of dimers in adjacent protofilaments is that observed in the A-tubule of flagellar doublet microtubules (Amos & Klug, 1974) and is assumed to occur also in normal brain microtubules, since it is the only symmetrical arrangement possible in a 13-protofilament tubule. This will be discussed in more detail elsewhere (Amos, 1978). As a result, the nearest interprotofilament contacts (along the 3-start direction) are between monomers of different types. The bonding regions in Fig. 4(a) would, however, match up equally well with contacts between like monomers.

the minimum zinc concentrations required for the formation of Zn-induced sheets (see Larsson *et al.*, 1976 and also Materials and Methods, section (a)) it is likely that a zinc ion is needed to bind to each tubulin monomer in order to directly or indirectly form the interprotofilament bonds.

The fact that apparently similar protofilaments are common elements in such different structures reinforces the concept of the protofilament as an entity, supporting the idea that the protofilament is an intermediate structure in tubulin polymerization (Erickson, 1974b; Kirschner *et al.*, 1974) and that the rings produced by disassembly consist of rolled-up protofilaments. The new images confirm earlier impressions that the intraprotofilament bonds are significantly stronger than the interprotofilament bonds.

The resolution is sufficient to see subunits with distinct shapes. The two kinds of subunits have similar asymmetric outlines and appear to be in approximately the



same orientation. This eliminates the possibility that the dimer might have an approximate dyad; i.e. the dimer, as well as the monomers, is definitely polar. As a result, the question posed by Erickson (1974a) of how the dimer is divided into two subunits now seems to be resolved; because of the polar shape of the morphological units, revealed in our images and in the normal sheet image of Crepeau *et al.* (1977), it seems unlikely that the dimer can consist of two similar, narrow, 82 Å long subunits, placed side-by-side. It seems almost certain that the tubulin monomers correspond to the globular subunits, as represented by Amos & Klug (1974). It is difficult to draw any firm conclusions from the difference in appearance between  $\alpha$  and  $\beta$ , even though the differences are distinct and reproducible. Are they really significantly different in internal structure because of the extensive differences in amino acid sequence, or are they similar but viewed from different orientations? It is impossible to distinguish between these two possibilities from a single projection of the structure. Three-dimensional information is necessary to resolve this question.

We thank Drs R. Henderson, P. N. T. Unwin and A. Klug for helpful discussions, and C. Harley for providing the TMV sample. One of the authors (T. S. B.) is a Fellow of the Jane Coffin Childs Memorial Fund for Medical Research. This investigation has been aided by a grant from the Jane Coffin Childs Memorial Fund for Medical Research.

## REFERENCES

- Aebi, U., Smith, P. R., Dubochet, J., Henry, C. & Kellenberger, E. (1973). *J. Supramol. Struct.* **1**, 498–522.
- Amos, L. A. (1977). *J. Cell Biol.* **72**, 642–654.
- Amos, L. A. (1978). In *Microtubules* (Roberts, K. & Hyams, J. S., eds), Academic Press Inc., London, in the press.
- Amos, L. A. & Klug, A. (1974). *J. Cell Sci.* **14**, 523–549.
- Amos, L. A., Linck, R. W. & Klug, A. (1976). *Cold Spring Harbor Conf. on Cell Proliferation*, **3**, *Cell Motility*, pp. 847–867.
- Arndt, U. W., Crowther, R. A. & Mallet, J. F. W. (1968). *J. Scient. Instrum.* (2) **1**, 510–516.
- Borisy, G. G., Mareum, J. M., Olmsted, J. B., Murphy, D. B. & Johnson, K. A. (1975). *Ann. N.Y. Acad. Sci.* **253**, 107–132.
- Bryan, J. & Wilson, L. (1971). *Proc. Nat. Acad. Sci., U.S.A.* **68**, 1762–1766.
- Cohen, C., DeRosier, D., Harrison, S. C., Stephens, R. E. & Thomas, J. (1975). *Ann. N.Y. Acad. Sci.* **253**, 53–59.
- Crepeau, R. H., McEwen, B., Dykes, G. & Edelstein, S. J. (1977). *J. Mol. Biol.* **116**, 301–315.
- Dentler, W. L., Granett, S. & Rosenbaum, J. L. (1975). *J. Cell Biol.* **65**, 237–241.
- DeRosier, D. J. & Klug, A. (1972). *J. Mol. Biol.* **65**, 469–488.
- Erickson, H. P. (1974a). *J. Cell Biol.* **60**, 153–167.
- Erickson, H. P. (1974b). *J. Supramol. Struct.* **2**, 393–411.
- Erickson, H. P. & Klug, A. (1971). *Phil. Trans. Roy. Soc. ser. B*, **261**, 105–118.
- Finch, J. T., Klug, A. & Nermut, M. V. (1967). *J. Cell Sci.* **2**, 587–590.
- Gaskin, F. & Kress, Y. (1977). *J. Biol. Chem.* **252**, 6918–6924.
- Glaeser, R. M. (1971). *J. Ultrastruct. Res.* **36**, 466–482.
- Grimstone, A. V. & Klug, A. (1966). *J. Cell Sci.* **1**, 351–362.
- Huxley, H. E. & Zubay, G. (1960). *J. Mol. Biol.* **2**, 10–18.
- Kirsehner, M. W., Williams, R. C., Weingarten, M. & Gerhart, J. C. (1974). *Proc. Nat. Acad. Sci., U.S.A.* **71**, 1159–1163.
- Kuo, I. A. M. & Glaeser, R. M. (1975). *Ultramic.* **1**, 53–66.
- Larsson, H., Wallin, M. & Edstrom, A. (1976). *Exp. Cell Res.* **100**, 104–110.
- Linck, R. W. (1976). *J. Cell Sci.* **20**, 405–439.
- Luduena, R. F. & Woodward, D. O. (1973). *Proc. Nat. Acad. Sci., U.S.A.* **70**, 3594–3598.

- Luduena, R. F., Shooter, E. M. & Wilson, L. (1977). *J. Biol. Chem.* **252**, 7006-7014.
- Mandelkow, E., Thomas, J. & Cohen, C. (1977). *Proc. Nat. Acad. Sci., U.S.A.* **74**, 3370-3374.
- Murphy, D. B. & Borisy, G. G. (1975). *Proc. Nat. Acad. Sci., U.S.A.* **72**, 2696-2700.
- Olmsted, J. B., Witman, G. B., Carlson, K. & Rosenbaum, J. (1971). *Proc. Nat. Acad. Sci., U.S.A.* **68**, 2273-2277.
- Piperno, G., Huang, B. & Luck, D. J. L. (1977). *Proc. Nat. Acad. Sci., U.S.A.* **74**, 1600-1604.
- Shelanski, M. L., Gaskin, F. & Cantor, C. R. (1973). *Proc. Nat. Acad. Sci., U.S.A.* **70**, 765-768.
- Sloboda, R. D., Rudolph, S. A., Rosenbaum, J. L. & Greengard, P. (1975). *Proc. Nat. Acad. Sci., U.S.A.* **72**, 177-181.
- Snyder, J. A. & McIntosh, J. R. (1976). *Annu. Rev. Biochem.* **45**, 699-720.
- Tsuprun, V. L., Stel'mashuk, V. Ya., Kiselev, N. A., Gel'fand, V. I. & Rozenblat, V. A. (1975). *Mol. Biol.* (translated from Russian), **10**, 360-367.
- Unwin, P. N. T. (1974). *J. Mol. Biol.* **87**, 657-670.
- Unwin, P. N. T. & Henderson, R. (1975). *J. Mol. Biol.* **94**, 425-440.
- Vallee, R. B. & Borisy, G. G. (1977). *J. Biol. Chem.* **252**, 377-382.
- Wallin, M., Larsson, H. & Edstrom, A. (1977). *Exp. Cell Res.* **107**, 219-225.
- Williams, R. C. & Fisher, H. W. (1970). *J. Mol. Biol.* **52**, 121-123.